ORIGINAL RESEARCH Open access

A Multi-Resolution Remote Sensing Approach for Water Hyacinth Detection in Aquatic Ecosystems

Carlos Oliveira[1*], Ana Santos[1], Rafael Costa[2], Beatriz Souza[3]

Abstract

Robust procedures for detecting and tracking invasive plant species are essential. Addressing these plants in aquatic ecosystems is particularly significant, given their potential to disrupt biodiversity and, in turn, impair overall ecosystem functioning and the services it provides. The present study focuses on identifying water hyacinth (Eichhornia crassipes) through multispectral imagery featuring distinct spatial resolutions. To achieve this, very high-resolution data (< 0.1 m) collected via an unmanned aerial vehicle (UAV) and lower-resolution data (10 m) sourced from Sentinel-2 MSI were employed. Three zones exhibiting substantial water hyacinth presence in the Lower Mondego region (Portugal) underwent UAV surveys. Various classification algorithms were tested for pixel-level identification of the invasive species across both image sources. Among the classifiers evaluated, random forest delivered the strongest performance (overall accuracy (OA): 0.94). Conversely, support vector machine yielded the lowest results (OA: 0.87), trailed by Gaussian naive Bayes (OA: 0.88), k-nearest neighbours (OA: 0.90), and artificial neural networks (OA: 0.91). Thanks to the superior spatial detail of UAV imagery, even minor patches of water hyacinth could be detected—patches that were undetectable in Sentinel-2 imagery. Even with its reduced resolution, the satellite-based analysis successfully delineated water hyacinth coverage, aligning closely with UAV findings. Integrating the two data sources while accounting for their resolution differences enabled clear tracking of the temporal and spatial progression of water hyacinth. This strategy demonstrated strong effectiveness in evaluating the outcomes of mitigation and control actions applied within the study zones. Consequently, the method provides a reliable means to identify invasive species in water bodies and monitor their development over time.

Keywords Machine learning, Unmanned aerial vehicles, Invasive species, Sentinel-2, Multitemporal analysis

*Correspondence:
Carlos Oliveira
carlos.oliveira@ufv.br
[1] Department of AI for Coffee Leaf Rust and Berry Borer Prediction using Satellite Data, Faculty of Agriculture, Federal University of Viçosa, Viçosa, Brazil
[2] Department of Machine Learning for Soil Organic Carbon Stock Estimation, Faculty of Agriculture, University of Campinas, Campinas, Brazil
[3] Department of Smart Harvesting Route Optimization, Faculty of Agriculture, University of São Paulo, São Paulo, Brazil

Introduction

Invasive alien species (IAS) rank among the most serious risks to biodiversity and the sustained provision of ecosystem services [1]. Beyond their harmful effects on the environment, IAS also causes significant social and economic losses by reducing productivity in sectors such as agriculture, forestry, fisheries, and tourism. Even though only a limited share of introduced species become invasive, the annual economic harm they cause exceeds EUR 10 billion [2]. Overall, invasive species imposed total costs of EUR 116.61 billion in Europe from 1960 to 2020, the bulk (60%) stemming from direct damage across various industries [3]. In freshwater systems, IAS can drive individual species to extinction, profoundly reshape native community structures, and modify key ecosystem processes [4, 5].

This is an open access article distributed under the terms of the Creative Commons Attribution-NonCommercial-ShareAlike 4.0 International License (CC BY-NC-SA 4.0), which permits non-commercial use, distribution, reproduction, and adaptation in any medium or format, provided that appropriate credit is given to the original author(s) and source, a link to the license is provided, and any changes made are indicated. Adapted material must be distributed under the same license.

© 2026 The Author(s). | Published by Agro Intelligence Research Press

Water hyacinth (Eichhornia crassipes) is among the most aggressive and common invasive aquatic plants. It is also ranked among the world's top 100 exotic species with the greatest invasion potential [6]. Originating in the Amazon basin, it began expanding worldwide in the late 19th century due to its popularity as an ornamental plant and now occurs on every continent except Antarctica [7, 8]. The species thrives in still-water environments, though its growth is constrained by low nutrient availability, water temperatures under 10 °C, and elevated salinity. As a result, nutrient-rich lakes, ponds, reservoirs, downstream river sections, and irrigation channels situated below 40° N and S latitude face the highest risk. Within Europe, its spread remains confined mainly to southern countries: Portugal, Spain, Italy, and France (Corsica) [8]. In Portugal, water hyacinth was first observed in 1939 within the Tagus basin [9] and has since spread across nearly all mainland areas ("Minho", "Douro Litoral", "Beira Litoral", "Estremadura e Ribatejo", "Alentejo", and "Algarve"), including the Azores island of "Terceira" [9-11].

Eichhornia crassipes reproduces both vegetatively—through fast clonal propagation—and sexually, by generating abundant seeds. This dual strategy grants it a strong competitive edge against native macrophytes in colonized habitats [8, 12]. Fragments produced by vegetative growth can endure cold periods and are transported by water currents and wind, sparking new invasion sites at different distances from the source population [13]. In heavily invaded sites, the plant develops dense floating mats that blanket water surfaces, triggering major ecological disruptions. These include sharp declines in phytoplankton, zooplankton, macroinvertebrates, and fish populations due to reduced light availability, lower dissolved oxygen levels, higher turbidity, poorer water quality, and the displacement of indigenous aquatic plants.

Furthermore, it impedes irrigation channels and navigation routes, with negative consequences for water supply, boating, fishing, farming, tourism, and hydropower facilities through turbine blockages [7, 8, 14-16]. Eradicating water hyacinth after establishment proves extremely challenging [14]. For this reason, management strategies typically concentrate on reducing financial losses and limiting ecological harm [7, 8].

Remote sensing techniques for separating water hyacinth from other floating or submerged plants, especially via satellite images, have been examined by multiple researchers [17]. Landsat 8 and Sentinel-2 datasets are favored in many cases owing to their open access and strong spectral, temporal, and spatial capabilities [18]. A large proportion of recent work applies supervised pixel-based classification of multispectral images supported by machine learning (ML) methods, including random forests (RFs), support vector machines (SVMs), artificial neural networks (ANNs), and related approaches [14, 16, 17]. Damtie *et al.* [19] investigated how this invasive plant influences evapotranspiration in Lake Tana (Ethiopia) using Sentinel-2 data. Mukarugwiro *et al.* [20] mapped the distribution of water hyacinth in Rwandan water bodies using Landsat 8 imagery. Dube *et al.* [21] effectively differentiated invasive aquatic plants from native ones at Lake Manyame (Zimbabwe). Sentinel-2's finer 10 m resolution, relative to Landsat 8's 30 m, creates valuable opportunities for tracking invasion spread along rivers and confined waterways [21, 22]. Ghoussein *et al.* [23] used a fractional vegetation cover (FVC)-based method [24] and the soil-adjusted vegetation index (SAVI) [25] derived from Sentinel-2 time series to study water hyacinth dynamics over 4 years in the Al Kabir River (Lebanon). Datta *et al.* [17] also anticipated substantial benefits from merging traditional and advanced ML methods for image processing, particularly when paired with aerial data from affordable unmanned aerial vehicles (UAVs) equipped with digital cameras, a point supported by subsequent research [26]. Using UAVs instead of GPS-equipped dinghies, as described in Mukarugwiro *et al.* [20], for acquiring training and validation samples offers clear field advantages. Identical classifiers can process multispectral data from UAV sensors, whose capabilities continue to advance. For example, the MicaSense RedEdge-MX multispectral sensor [27] achieves a ground sample distance (GSD) of 8 cm per band at an altitude of 120 m. Benjamin *et al.* [28] applied this sensor to evaluate management success for a floating-leaved invasive plant in Palm Beach County (USA), boosting classification accuracy via vegetation indices (normalized difference vegetation index (NDVI) [29], visible-band difference vegetation index (VDVI) [30], and visible brightness (VB)). The literature contains many documented successes in using UAV sensors for terrestrial or aquatic vegetation research, either independently (with multispectral sensors and indices) or alongside satellite and ground observations [31]. UAV platforms have likewise demonstrated value in providing training and validation data to enhance satellite-based studies [20].

© 2026 The Author(s). | Published by Agro Intelligence Research Press

As far as the authors are aware, comparable methodologies have not yet been applied to water hyacinth detection. This work examined how well different ML classifiers could separate water hyacinth presence/absence in UAV and satellite multispectral datasets. It further evaluated whether merging UAV and satellite information could effectively track temporal changes in water hyacinth coverage, thereby clarifying the respective advantages and drawbacks of each platform. Accordingly, the current study specifically addresses two research questions: (1) Can water hyacinth infestations be identified with high accuracy by using coarse- and high-resolution multispectral data together in a complementary fashion? (2) If yes, is it feasible to monitor the temporal patterns of these infestations through the integration of UAV and satellite multispectral data?

Materials and Methods

Study area

The investigated region lies within the Mondego River basin **(Figure 1b)**, spanning the area between Coimbra and Figueira da Foz (Portugal). Water hyacinth infestation has grown especially severe in this zone during the past 4–5 years [16]. Three sites showing dense water hyacinth occurrence were chosen for UAV surveys (positions indicated in **Figure 1**). In addition to water hyacinth and open water, the sites include riparian trees, farmland, additional aquatic plants, general vegetation, roads, and various infrastructures **(Figures 1d and 1e)**. Area 1 comprises two water canals: a central one extending from the north and an eastern canal that joins before flowing into the primary Mondego River channel. Area 2 occupies the northern canal, which continues from Area 1, and features a secondary branch canal. Area 3 lies farther from the first two areas and contains the eastern canal that discharges into Area 1.

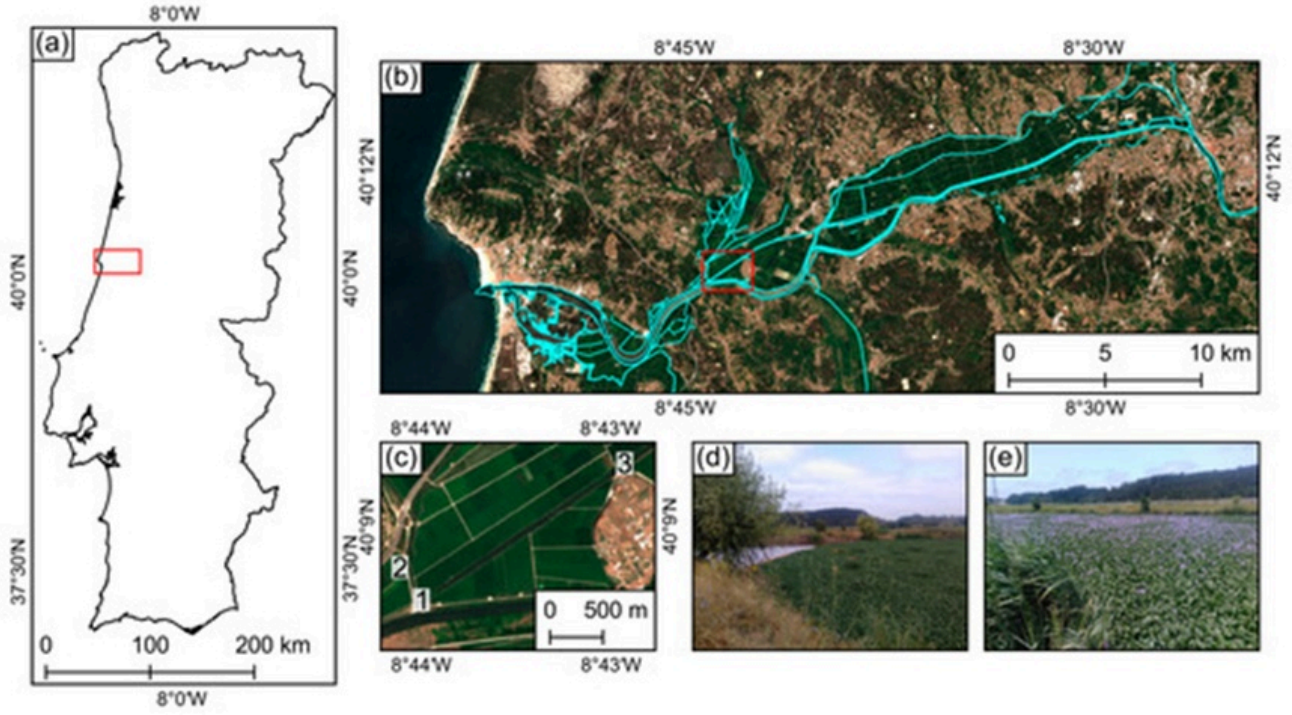


Figure 1. Overview of the study area: (a) its location within mainland Portugal, (b) overview of the Lower Mondego main water canals (in blue), (c) location of the three analysed areas, red polygon highlighted in (b); and (d, e) photographs of study areas 1 and 2, respectively.

Remotely sensed data

Unmanned aerial vehicle and data acquisition

© 2026 The Author(s). | Published by Agro Intelligence Research Press

The Matrice 300 RTK (DJI, Shenzhen, China) served as the unmanned aerial platform for obtaining very detailed spatial data. This four-rotor UAV included real-time kinematic (RTK) positioning, weighed roughly 6.3 kg when fitted with its two power batteries, and supported payloads up to 2.7 kg. The MicaSense RedEdge-MX (MicaSense, Inc.; Seattle, DC, USA) sensor handled data recording. This lightweight device (around 232 g) gathered information at 1280 × 960 resolution (1.2 megapixels) through five separate spectral ranges: blue (475 nm, 20 nm bandwidth), green (560 nm, 20 nm bandwidth), red (668 nm, 10 nm bandwidth), red edge (717 nm, 10 nm bandwidth), and near infrared (842 nm, 40 nm bandwidth). Mounted atop the UAV, a downwelling light sensor 2 (DLS 2) gathered incoming solar radiation while airborne. It captured ambient illumination and solar angles for all five bands, storing these details directly in image metadata files. Such records later helped adjust for shifts in overall lighting conditions mid-flight. The DLS 2 also delivered GPS coordinates to the MicaSense RedEdge-MX for accurate image positioning.

Three separate UAV missions took place on 21 July 2021, covering one study area each. Flights were conducted at 100 m altitude, resulting in a ground resolution of roughly 0.07 m — appropriate for the required precision and within the 120 m regulatory ceiling. Captured images maintained 80% forward overlap and 70% side overlap. A calibration target was prepared radiometrically for the sensor before each mission. Additional mission specifics appear in **Table 1**.

Table 1. Flight-campaign information for multispectral data acquired from the unmanned aerial vehicle.

Study area	Coordinates (Lat., Long.)	Altitude (m)	Start time	Covered area (ha)	Spatial resolution (cm)	No. of images (No. of captures)
1	40°8′55″ N 8°44′12″ W	0	10:35	23.3	7.35	1955 (391)
2	40°9′60″ N 8°44′17″ W	2	11:29	10.6	7.25	1135 (227)
3	40°9′38″ N 8°42′47″ W	4	14:06	8.9	7.24	910 (182)

Satellite data

This research also incorporated imagery from the Sentinel-2 Multispectral Instrument (MSI). Among its 13 spectral bands (B#), the selected ones were B2 (490 nm), B3 (560 nm), B4 (665 nm), B5 (705 nm), and B8 (842 nm), aligning with blue, green, red, red edge, and NIR ranges. Spatial resolution stood at 10 m for B2, B3, B4, and B8, but 20 m for B5. Resampling adjusted B5 to 10 m for uniformity.

Level-2A bottom-of-atmosphere products were retrieved for cloud-free scenes covering bands B2, B3, B4, B8, and B5, both preceding and following the UAV flights, together with true color composite (TCI) visuals. This led to the selection of Sentinel-2 MSI acquisitions on 13 July and 28 July 2021 — 8 days prior and 7 days after the UAV operations.

UAV data processing

Photogrammetry steps were necessary to prepare UAV flight images for further examination. Processing relied on Pix4Dmapper Pro software (Pix4D SA, Lausanne, Switzerland) for each location's dataset. Tie points were first matched between overlapping images using positional data and camera calibration details. Dense point clouds then emerged from this alignment. Inverse distance weighting (IDW) interpolation converted these into orthorectified layers, delivering calibrated reflectance maps for the five MicaSense RedEdge-MX bands. Although digital elevation models were produced, they were excluded from classification work because they were incompatible with the project goals. QGIS software merged the five bands into a single raster file. Band combinations then enabled multiple-color displays, notably

© 2026 The Author(s). | Published by Agro Intelligence Research Press

RGB orthomosaics **(Figure 2)**. These RGB versions drew from the red, green, and blue channels, standardized by setting the lowest reflectance across bands as the floor and each band's peak reflectance as the ceiling.

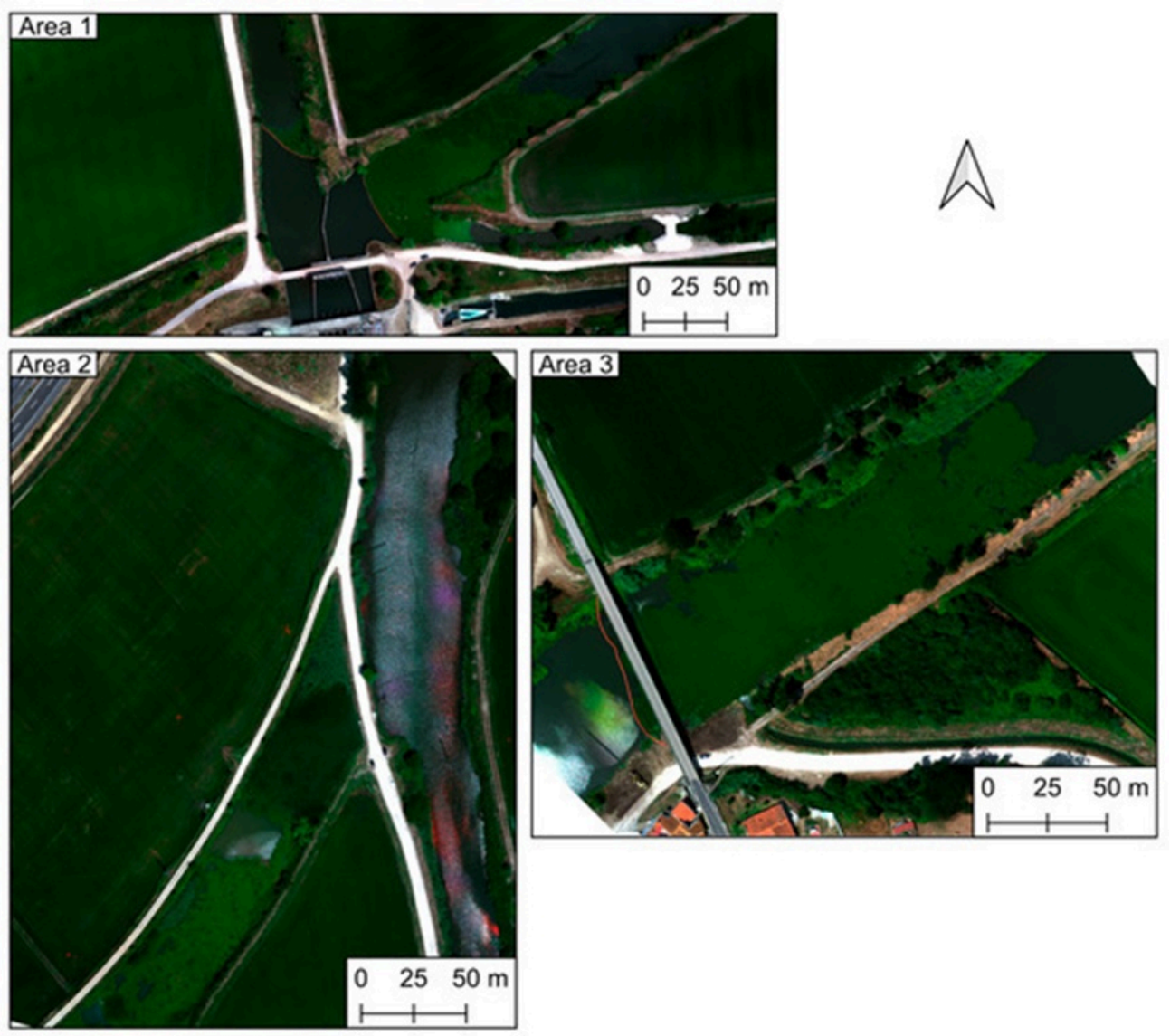


Figure 2. Red, green, blue (RGB) composite representation of the orthorectified multispectral data acquired by an unmanned aerial vehicle in the three study areas.

Water hyacinth classification procedure

Machine learning techniques enabled automated pixel-wise separation of water hyacinth based on spectral information. Supervised algorithms tested included RF, SVM, ANN, Gaussian naive Bayes (NB), and k-nearest neighbours (KNN). RF parameters comprised a maximum depth of five, at least 10 samples per node, up to 100 trees, and 0.01 out-of-bag (OOB) error. SVM was trained with a linear kernel and a cost parameter C set to 1 [32]. ANN training applied resilient backpropagation [33], with five neurons per hidden layer, symmetrical sigmoid activation (alpha and beta both set to 1), and stopping rules of either 1000 iterations or 0.01 epsilon. KNN operated with 32 neighbours.

Training for supervised models demanded labeled examples. A robust dataset was assembled, comprising 100 polygons across the three zones: 50 confined to pure water hyacinth coverage and 50 covering mixed features such as open water,

© 2026 The Author(s). | Published by Agro Intelligence Research Press

roads, additional plants, and built structures. Twenty random points (each representing one pixel) were drawn per polygon, generating 2000 total points (658 in area 1, 881 in area 2, 461 in area 3). Water hyacinth pixels were labeled as class 1; all others were labeled as class 0. The Sentinel-2 MSI portion used 100 balanced points (50 per class) from the three zones (40 from area 1, 31 from area 2, 29 from area 3). Samples are split into 70% for training and 30% for testing. Input features consisted of reflectance from the five bands (blue, green, red, red edge, NIR). Class distribution stayed evenly balanced.

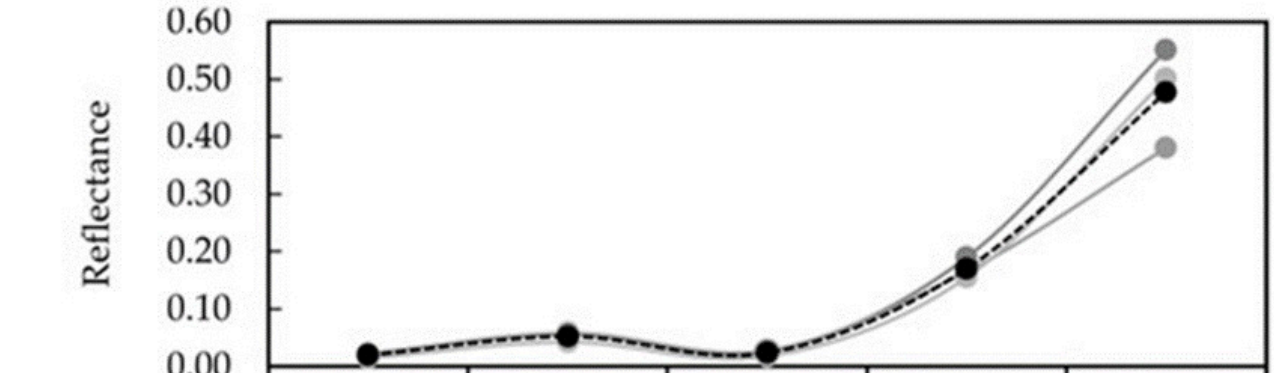
Performance evaluation was based on confusion matrix outputs on the held-out test set, yielding user's accuracy (UA), producer's accuracy (PA), kappa coefficient (K), and overall accuracy (OA). Kappa values were interpreted according to Landis and Koch's intervals [34]. Further metric explanations are available in Barsi *et al.* [35].

Training and validation covered all three zones with UAV imagery plus Sentinel-2 MSI records dated 28 July 2021. Final classifications also tested an input mask to check performance for water hyacinth mapping when extending beyond river channels alone.

Results and Discussion

Dataset characterization

Spectral signatures of water hyacinth were profiled by placing 25 polygons of 0.5 m × 0.5 m size in each study zone and checking for inter-site reflectance variations. Mean pixel values per polygon were computed band by band **(Figure 3)**.



	Blue	Green	Red	Red edge	NIR
Area 1	0.02	0.06	0.03	0.19	0.55
Area 2	0.02	0.06	0.03	0.17	0.38
Area 3	0.01	0.04	0.02	0.16	0.50
All	0.02	0.05	0.02	0.17	0.48

Figure 3. Average reflectance of water hyacinth samples in the three surveyed areas for the five bands acquired by the MicaSense RedEdge-MX sensor with the unmanned aerial vehicle.

The largest divergence occurred in the NIR band, showing reduced reflectance in the second zone. Flowering conditions in parts of that zone likely contributed. The third zone displayed modestly lower values in the blue, green, and red edge bands relative to its counterparts. Across all 75 polygons, reflectance rose from blue to green, dipped in red, and climbed sharply in red edge and NIR. Such a response matched expectations for vegetation holding moderate leaf cover.

© 2026 The Author(s). | Published by Agro Intelligence Research Press

Classification performance of each classifier

Outcomes from trained classifiers distinguishing water hyacinth from surrounding features **(Figure 1c)** are reviewed here.

UAV multispectral results **(Table 2)** indicated solid OA above 85% for every algorithm. SVM scored the lowest at 87%, while RF achieved the highest at 94%. Classifier ranking remained consistent across K evaluations. SVM and NB alone remained below 0.8 (still reasonable agreement), whereas the remaining models achieved high concordance, peaking at 0.88 K for RF. UA and PA for pixel-level water hyacinth detection revealed more frequent false positives than false negatives. RF excelled in both accuracy types.

Table 2. Validation of models created by different classifiers using data acquired by an unmanned aerial vehicle and from Sentinel-2 MSI. The best result in each metric and platform is highlighted in bold. UA: user's accuracy; PA: producer's accuracy; K: kappa coefficient; OA: overall accuracy; RF: random forest; SVM: support vector machine; ANN: artificial neural network; NB: Gaussian naive Bayes; KNN: k-nearest neighbors.

Classifier	UA	PA	K	OA
Unmanned aerial vehicle data				
RF	0.93	0.96	0.88	0.94
SVM	0.83	0.93	0.74	0.87
ANN	0.87	0.96	0.82	0.91
NB	0.82	0.98	0.77	0.88
KNN	0.88	0.93	0.81	0.90
Sentinel-2 data				
RF	0.88	0.93	0.80	0.90
SVM	1.00	0.67	0.67	0.83
ANN	0.93	0.87	0.80	0.90
NB	1.00	0.73	0.73	0.87
KNN	0.92	0.80	0.73	0.87

Sentinel-2 MSI classification **(Table 2)** produced OA between 83% (SVM) and 90% (RF and ANN), with NB and KNN at 87%. K values tracked OA closely: 0.67 for SVM, 0.73 for NB and KNN, and 0.80 for the rest. UA for class 1 typically surpassed PA, except under RF.

Prediction of water hyacinth dispersion

While all classifiers performed acceptably on both data types, RF performed best across most indicators **(Table 2)**, with minimal misclassifications. RF, therefore, mapped the extent of water hyacinth. Mapping outputs for UAV (21 July) and Sentinel-2 (28 July) appear in **Figure 4**. Detection succeeded overall, including some detections outside channels on both platforms.

© 2026 The Author(s). | Published by Agro Intelligence Research Press

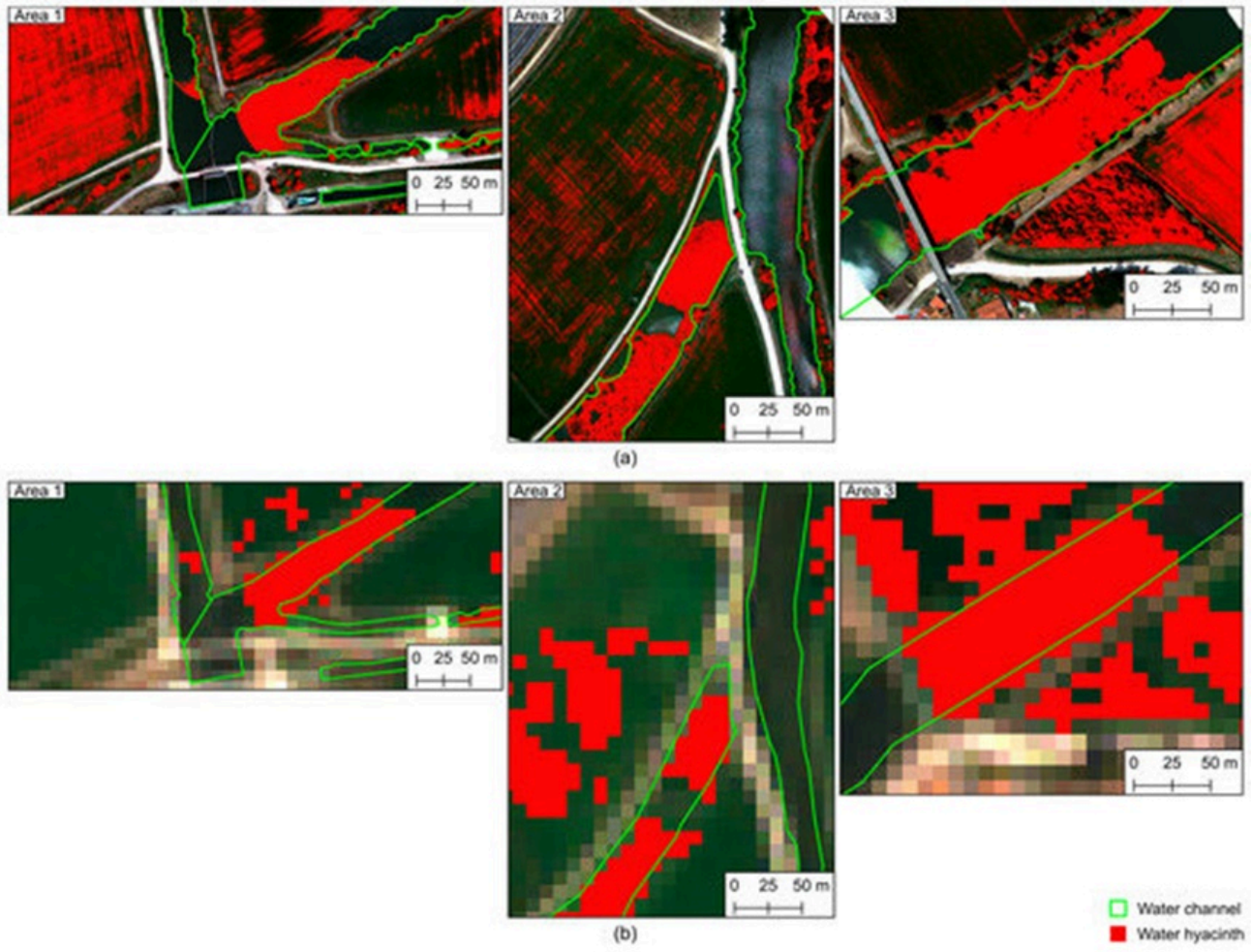


Figure 4. Classification of water hyacinth in the three study areas using multispectral data from an unmanned aerial vehicle (a) and from Sentinel-2 (b).

Channel-restricted masking narrowed the focus to aquatic pathways for temporal-spread assessment. RF models from UAV and Sentinel-2 sources examined coverage shifts on 13 July 2021 (pre-UAV), 21 July 2021 (UAV date), and 28 July 2021 (post-UAV), with flanking dates from Sentinel-2 MSI .**Figure 5** displays outcomes. Spatial patterns varied noticeably. Area 1 showed shifting accumulations between 13–21 July, especially in the central channel (absent on 13 July) and near the outlet to the Mondego River. Minimal further shifts occurred by 28 July. Area 2, flowering during UAV acquisition, showed changes from 13–21 July, with a heavy concentration in the side channel. Area 3 showed a steady buildup over time.

© 2026 The Author(s). | Published by Agro Intelligence Research Press

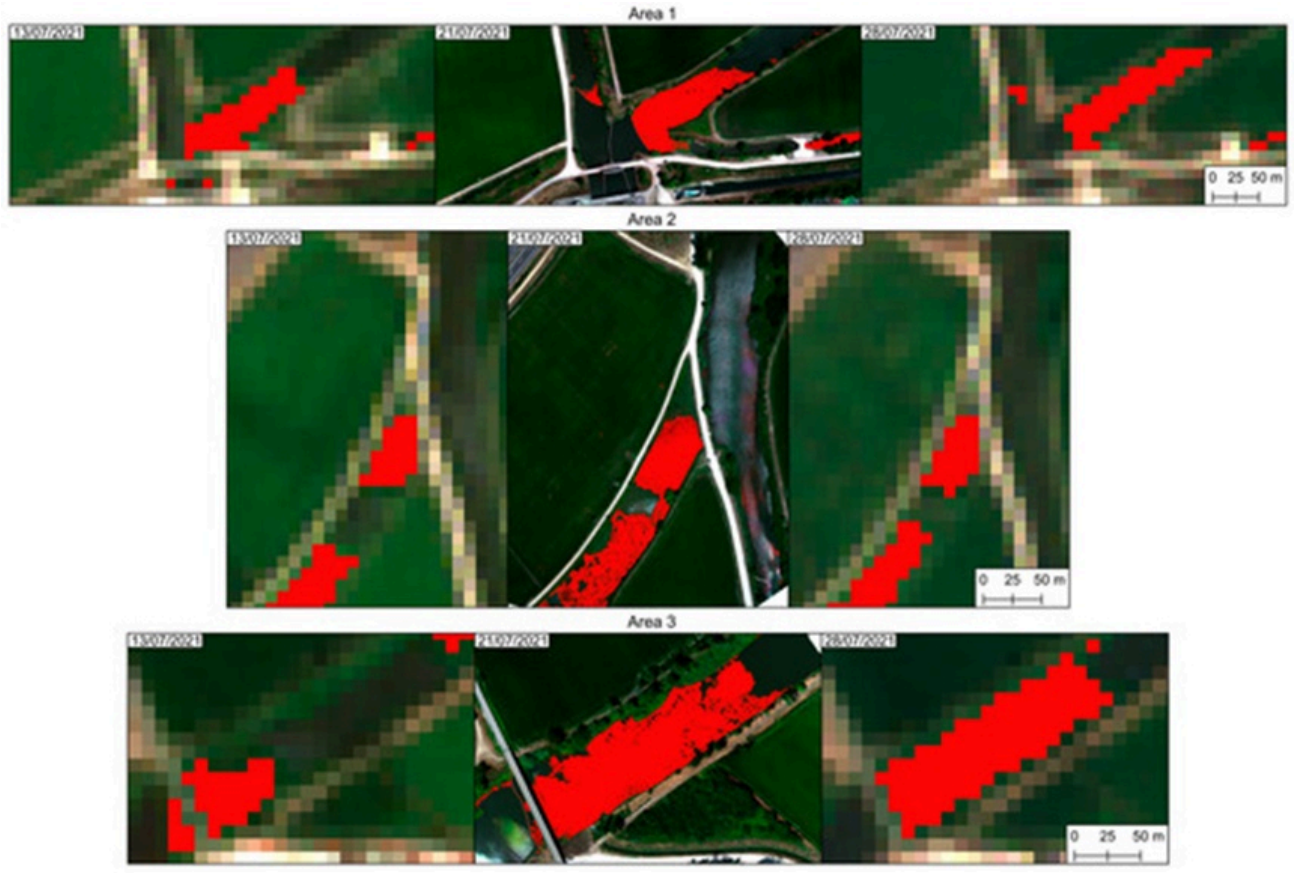


Figure 5. Water hyacinth coverage in the water channels of the surveyed areas on three consecutive dates. Red pixels mark the potential presence of water hyacinth.

Dispersion patterns **(Figure 5)** uncovered coverage fluctuations. **Table 3** summarizes occupation percentages, revealing varied trends. Every zone maintained at least 20% cover of invasive plants. Area 1 grew by about 1% initially, then by 4% later (expanding from 5300 m² to 6400 m²). Area 2 rose from 22% to 29% before falling by 4%. Area 3 posted the biggest jump at 27% from 13–21 July, then eased 1% by 28 July.

Table 3. Water hyacinth surface coverage estimation over time in the analyzed areas.

Study Area	Estimated surface (m^2)			Total surface (m^2)
	13 July 2021	21 July 2021	28 July 2021	
1	5300	5524	6400	20,777
2	4100	5438	4700	18,790
3	3900	8699	8600	18,250

The review of the reflectance signatures captured from UAV multispectral imagery **(Figure 3)** confirms alignment with standard patterns observed in green vegetation with moderate leaf coverage [36]. The noted NIR reflectance variations in study area 2 are likely due to many plants being in bloom there **(Figure 1e)**.

Outcomes for the classifiers applied to UAV data identified RF as delivering superior accuracy, whereas SVM registered the poorest showing. On the Sentinel-2 side, various algorithms produced OA figures that closely matched and had

© 2026 The Author(s). | Published by Agro Intelligence Research Press

narrower gaps between the two categories. The side-by-side evaluation of UAV results against Sentinel-2 **(Table 2)** demonstrates markedly stronger outcomes from the UAV multispectral records. Contributing factors include the substantially larger sample pool fed into UAV models (2000 versus 100 for Sentinel-2) and the 10 m pixel size of Sentinel-2 imagery, which often blends signals from multiple surface types within a single pixel [37]. As a result, pixels containing sparse water hyacinth portions are more likely to be misassigned. Even so, the accuracies achieved correspond well with findings from earlier publications. Damtie *et al.* [19] reported OA of 95.1%-99.7% and K values of 0.93–0.97 using maximum likelihood processing of Sentinel-2 MSI. Mukarugwiro *et al.* [20] secured OA of 85% (k = 0.81) via RF on Landsat 8 imagery, surpassing SVM (OA of 65%; k = 0.57), while Dube *et al.* [21] attained OA of 92% employing two ML ensemble techniques along with discriminant analysis (DA) and partial least squares discriminant analysis (PLS-DA). Using UAV multispectral imagery, Chabot *et al.* [38] deployed RF to observe emergent (OA of 92%; k = 0.88) and submerged (OA of 84%; k = 0.75) invasive water plants in shallow settings.

Selection fell on RF due to its leading performance, and it was subsequently applied to map water hyacinth occurrence in the target zones **(Figures 4 and 5)**. Mapped outputs proved reliable during mask application, allowing RF to spot major concentrations and detect thinner stands distributed along the channels. Blooming vegetation in study area 2 posed no hindrance and was properly identified. The absence of a restricting mask around water channels alone **(Figure 4)**—the exclusive environment for water hyacinth—led to excessive detections. UAV records incorrectly signaled water hyacinth amid farmland (across all zones) and within tree cover (areas 1 and 3). Spectral overlap is a plausible cause, given that rice fields prevail in the Lower Mondego River basin [39, 40] and exhibit partial water integration [41]. Parallel issues emerged in Sentinel-2 MSI mappings, except that the western field of study area 1 escaped errors, while fields in the third zone had elevated error counts. Timing discrepancies across the source datasets explain these contrasts. Testing various vegetation indices holds promise for refinement, as mathematical band manipulations can accentuate relevant characteristics in focus zones [42]. Exploration of the shortwave infrared (SWIR) bands available in Sentinel-2 MSI also merits pursuit, as in Thamaga and Dube [43], who incorporated both indices and SWIR channels.

Portugal's 2030 National Strategy for Nature and Biodiversity Conservation (Resolução do Conselho de Ministros n.º 55/2018 [44]) rests on three principal pillars: upgrading the status of natural assets, heightening appreciation of their significance, and advancing public engagement with nature and biodiversity. Accordingly, entities overseeing biological management in canals linked to the Mondego River (Portugal) foster water hyacinth clustering through targeted floating barriers. These installations streamline mechanical collection operations and curb short-term effects of the IAS. The fusion of UAV and satellite information facilitated a chronological examination of water hyacinth expansion **(Figure 5; Table 3)**. This review uncovered shifts in position over time and documented field-based containment measures to address the IAS surge. Within study area 1, installation of two floating barriers at the exits of both canals occurred between 13 and 21 July, a change readily apparent in the classified maps; on 13 July, the westernmost channel displayed virtually zero buildup, restricted solely to the eastern channel. Following barrier placement, buildup formed farther from the exit points. In study area 2, the enhanced detail from UAV imagery revealed finer-scale fluctuations, including a central patch of water hyacinth undetectable with precision under Sentinel-2 MSI. This distinction potentially clarifies the recorded coverage reduction between 21 and 28 July. In study area 3, which also received a floating barrier, progressive plant buildup was evident over successive intervals. Moreover, its position midway in the canal draining toward study area 1 plausibly accounts for the minor decline in the latest interval. The substantial rise between the opening intervals may be linked to the barrier's deployment, which promotes collection, yet this interpretation requires additional confirmation.

Expanding the present work invites attention to several aspects that remain untouched. Continuous tracking of water hyacinth throughout the Lower Mondego can leverage the ongoing stream of Sentinel-2 MSI records, as in Ghoussein *et al.* [23]. Persistent observation efforts would thus measure the impact of deployed interventions against the IAS. During periods of highest activity, UAV multispectral acquisitions can usefully augment satellite imagery to confirm the results of physical extraction efforts, mirroring the approach in Lishawa *et al.* [45]. Fixed-wing UAVs provide decent coverage suitable for wetland studies in estuaries [46], yet multirotor variants offer greater benefits under these conditions [42].

© 2026 The Author(s). | Published by Agro Intelligence Research Press

Additionally, the potential for deriving water hyacinth biomass estimates from remote sensing inputs (chiefly UAV) remains open for study. Datta *et al.* [17] propose that remote sensing-based biomass appraisal of water bodies could enable profitable utilization as a primary management tool for water hyacinth, given the limitations of alternative tactics. Such direction holds strong potential for UAV deployment in localized checks that require frequent, high-detail imagery. UAV-mounted multispectral systems supply outstanding spatial, spectral, and temporal detail suited to observing water hyacinth proliferation in water environments [47], above all in narrower waterways under 10 m, since Sentinel-2 records suffer pixel mixing with surrounding terrain [48]. Case-by-case determination of ideal spatial resolution is advisable, since aggregated pixels may sometimes deliver superior classification balance compared with raw data [49].

Conclusion

The material presented in this manuscript describes investigative activities aimed at identifying and tracking the spread of water hyacinth in the Lower Mondego region (Portugal). Classification routines for this species applied to multispectral inputs gathered by UAV and satellite platforms—at sub-decimeter and decameter resolutions, respectively—established that RF-derived models yielded the best performance across both platforms. Although the two remote sensing sources differ in spatial detail, evidence indicates that monitoring this species' behavioral shifts remains achievable through satellite or UAV platforms, along with the assessment of field containment and mitigation initiatives currently in place.

Acknowledgements

None

Conflict of interest

None

Financial support

This research activity was funded by POCI-FEDER as part of the project "BioComp_2.0—Produção de compostos orgânicos biológicos para o controlo do jacinto de água e para a valorização de subprodutos agropecuários, florestais e agroindustriais" (POCI-01-0247-FEDER-070123) and by national funds through FCT (Portuguese Foundation for Science and Technology) under the projects UIDB/04033/2020 and UIDB/00690/2020.

Ethics statement

None

Received: 08 Nov 2024 Revised: 13 Jan 2025 Accepted: 29 Jan 2025
Published online: 25 November 2026

Rights and permissions

Open Access The author(s) retain copyright. This article is licensed under the Creative Commons Attribution-NonCommercial-ShareAlike 4.0 International License. It may be shared and adapted for non-commercial purposes with appropriate attribution, an indication of changes, and distribution of adaptations under the same license. Third-party material may be subject to separate terms identified in its credit line. View the license at https://creativecommons.org/licenses/by-nc-sa/4.0/.

References

1. Kass MJ. Summary for Policymakers of the Global Assessment Report on Biodiversity and Ecosystem Services. Nat Resour Environ. 2020;34:62.

2. Hulme PE, Pyšek P, Nentwig W, Vilà M. Will threat of biological invasions unite the European Union? Science. 2009;324:40–1.

3. Haubrock PJ, Turbelin AJ, Cuthbert RN, Novoa A, Taylor NG, Angulo E, et al. Economic costs of invasive alien species across Europe. NeoBiota. 2021;67:153–90.

4. Gallardo B, Clavero M, Sánchez MI, Vilà M. Global ecological impacts of invasive species in aquatic ecosystems. Glob Change Biol. 2016;22:151–63.

5. Cuthbert RN, Pattison Z, Taylor NG, Verbrugge L, Diagne C, Ahmed DA, et al. Global economic costs of aquatic invasive alien species. Sci Total Environ. 2021;775:145238.

6. Lowe S, Browne M, Boudjelas S, De Poorter M. 100 of the World's Worst Invasive Alien Species: A Selection from the Global Invasive Species Database. Auckland, New Zealand: Invasive Species Specialist Group Auckland; 2000; 12.

7. Kriticos DJ, Brunel S. Assessing and managing the current and future pest risk from water hyacinth (Eichhornia crassipes), an invasive aquatic plant threatening the environment and water security. PLoS ONE. 2016;11:e0120054.

8. Coetzee JA, Hill MP, Ruiz-Téllez T, Starfinger U, Brunel S. Monographs on invasive plants in Europe N° 2: Eichhornia crassipes (Mart.) Solms. Bot Lett. 2017;164:303–26.

9. Duarte C, Agusti S, Moreira I. Water hyacinth (Eichornia crassipes (Mart.) Solms) and water milfoil (Myriophyllum aquaticum Vell. Verde) in Portugal. In: Proceedings of the 3rd Symposium on Weed Problems in the Mediterranean Area; EWRS: Oeiras, Portugal;1984; 1. http://hdl.handle.net/10400.5/16306 (accessed on 30 December 2021).

10. Figueiredo J, Duarte C, Moreira I, Agusti S. As infestantes aquáticas nos sistemas de irrigação e drenagem do Ribatejo. Recur Hídricos. 1984;5:5–10.

11. Moreira I, Monteiro A, Ferreia M, Catarino L, Franco J, Rebelo T. Estudos sobre biologia e combate do jacinto aquático (Eichhornia crassipes (Mart. Solms-Laub.)) em Portugal. Garcia da Horta Série Botânica. 1999;14:191–8.

12. Albano Pérez E, Ruiz Téllez T, Sánchez Guzmán JM. Influence of physico-chemical parameters of the aquatic medium on germination of Eichhornia crassipes seeds. Plant Biol. 2011;13:643–8.

13. Téllez TR, López E, Granado GL, Pérez EA, López RM, Guzmán JMS. The water hyacinth, Eichhornia crassipes: An invasive plant in the Guadiana River Basin (Spain). Aquat Invasions. 2008;3:42–53.

14. Villamagna AM, Murphy BR. Ecological and socio-economic impacts of invasive water hyacinth (Eichhornia crassipes): A review. Freshw Biol. 2010;55:282–98.

15. Patel S. Threats, management and envisaged utilizations of aquatic weed Eichhornia crassipes: An overview. Rev Environ Sci Biotechnol. 2012;11:249–59.

16. Stratoudakis Y, Correia C, Belo AF, de Almeida PR. Improving participated management under poor fishers' organization: Anadromous fishing in the estuary of Mondego River, Portugal. Mar Policy. 2020;119:104049.

17. Datta A, Maharaj S, Prabhu GN, Bhowmik D, Marino A, Akbari V, et al. Monitoring the spread of water hyacinth (Pontederia crassipes): Challenges and future developments. Front Ecol Evol. 2021;9:6.

© 2026 The Author(s). | Published by Agro Intelligence Research Press

18. Pádua L, Guimarães N, Adão T, Sousa A, Peres E, Sousa JJ. Effectiveness of Sentinel-2 in multi-temporal post-fire monitoring when compared with UAV imagery. ISPRS Int J Geo-Inf. 2020;9:225.

19. Damtie YA, Mengistu DA, Meshesha DT. Spatial coverage of water hyacinth (Eichhornia crassipes (Mart.) Solms) on Lake Tana and associated water loss. Heliyon. 2021;7:e08196.

20. Mukarugwiro J, Newete S, Adam E, Nsanganwimana F, Abutaleb K, Byrne M. Mapping distribution of water hyacinth (Eichhornia crassipes) in Rwanda using multispectral remote sensing imagery. Afr J Aquat Sci. 2019;44:339–48.

21. Dube T, Mutanga O, Sibanda M, Bangamwabo V, Shoko C. Testing the detection and discrimination potential of the new Landsat 8 satellite data on the challenging water hyacinth (Eichhornia crassipes) in freshwater ecosystems. Appl Geogr. 2017;84:11–22.

22. Thamaga KH, Dube T. Remote sensing of invasive water hyacinth (Eichhornia crassipes): A review on applications and challenges. Remote Sens Appl Soc Environ. 2018;10:36–46.

23. Ghoussein Y, Nicolas H, Haury J, Fadel A, Pichelin P, Abou Hamdan H, et al. Multitemporal remote sensing based on an FVC reference period using Sentinel-2 for monitoring Eichhornia crassipes on a Mediterranean river. Remote Sens. 2019;11:1856.

24. Zhang X, Liao C, Li J, Sun Q. Fractional vegetation cover estimation in arid and semi-arid environments using HJ-1 satellite hyperspectral data. Int J Appl Earth Obs Geoinf. 2013;21:506–12.

25. Huete AR. A soil-adjusted vegetation index (SAVI). Remote Sens Environ. 1988;25:295–309.

26. Anker Y, Hershkovitz Y, Ben Dor E, Gasith A. Application of aerial digital photography for macrophyte cover and composition survey in small rural streams. River Res Appl. 2014;30:925–37.

27. MicaSense, Inc. The RedEdge-MX Sensor Data Sheet. https://micasense.com/wp-content/uploads/2019/11/Trifold-Dual-Camera-Product-Sheet.pdf (accessed on 12 December 2021).

28. Benjamin AR, Abd-Elrahman A, Gettys LA, Hochmair HH, Thayer K. Monitoring the efficacy of crested floatingheart (Nymphoides cristata) management with object-based image analysis of UAS imagery. Remote Sens. 2021;13:830.

29. Rouse JW Jr, Haas RH, Schell JA, Deering DW. Monitoring vegetation systems in the Great Plains with ERTS. In: Third Earth Resources Technology Satellite-1 Symposium: Section A; Scientific and Technical Information Office, National Aeronautics and Space Administration: Washington, DC, USA; 1973;1: 309–17.

30. Xiaoqin W, Miaomiao W, Shaoqiang W, Yundong W. Extraction of vegetation information from visible unmanned aerial vehicle images. Trans Chin Soc Agric Eng. 2015;31:152–9.

31. Gómez-Sapiens M, Schlatter KJ, Meléndez Á, Hernández-López D, Salazar H, Kendy E, et al. Improving the efficiency and accuracy of evaluating aridland riparian habitat restoration using unmanned aerial vehicles. Remote Sens Ecol Conserv. 2021;7:488–503.

32. Chang CC, Lin CJ. LIBSVM: A library for support vector machines. ACM Trans Intell Syst Technol. 2011;2:1–7.

33. Riedmiller M, Braun H. A direct adaptive method for faster backpropagation learning: The RPROP algorithm. IEEE Int Conf Neural Netw. 1993;1:586–91.

34. Landis JR, Koch GG. The measurement of observer agreement for categorical data. Biometrics. 1977;33:159–74.

35. Barsi Á, Kugler Z, László I, Szabó G, Abdulmutalib H. Accuracy dimensions in remote sensing. Int Arch Photogramm Remote Sens Spat Inf Sci. 2018;42.

© 2026 The Author(s). | Published by Agro Intelligence Research Press

36. Ling C, Liu H, Ju H, Zhang H, You J, Li W. A study on spectral signature analysis of wetland vegetation based on ground imaging spectrum data. J Phys Conf Ser. 2017;910:012045.

37. Traganos D, Reinartz P. Mapping Mediterranean seagrasses with Sentinel-2 imagery. Mar Pollut Bull. 2018;134:197–209.

38. Chabot D, Dillon C, Shemrock A, Weissflog N, Sager EPS. An object-based image analysis workflow for monitoring shallow-water aquatic vegetation in multispectral drone imagery. ISPRS Int J Geo-Inf. 2018;7:294.

39. Cunha M, Marques J, Azevedo J, Castilho A. Understanding the impact of a major hydro-agricultural project in Low Mondego area (Portugal). Land. 2021;10:114.

40. Marques JC, Graça MA, Pardal MÂ. Aquatic ecology of the Mondego River basin: Global importance of local experience. Coimbra, Portugal: Imprensa da Universidade de Coimbra; 2002. p. 7–12. ISBN 978-989-26-0336-0.

41. Ramadhani F, Pullanagari R, Kereszturi G, Procter J. Mapping of rice growth phases and bare land using Landsat-8 OLI with machine learning. Int J Remote Sens. 2020;41:8428–52.

42. Pádua L, Vanko J, Hruška J, Adão T, Sousa JJ, Peres E, et al. UAS, sensors, and data processing in agroforestry: A review towards practical applications. Int J Remote Sens. 2017;38:2349–91.

43. Thamaga KH, Dube T. Testing two methods for mapping water hyacinth (Eichhornia crassipes) in the Greater Letaba River System, South Africa: Discrimination and mapping potential of the polar-orbiting Sentinel-2 MSI and Landsat 8 OLI sensors. Int J Remote Sens. 2018;39:8041–59.

44. Presidência do Conselho de Ministros. Resolução do Conselho de Ministros no 55/2018. Diário Da República: I Série . 2018:1835–80. https://dre.pt/dre/detalhe/resolucao-conselho-ministros/55-2018-115226936 (accessed on 30 December 2021).

45. Lishawa SC, Carson BD, Brandt JS, Tallant JM, Reo NJ, Albert DA, et al. Mechanical harvesting effectively controls young Typha spp. invasion and unmanned aerial vehicle data enhances post-treatment monitoring. Front Plant Sci. 2017;8:619.

46. Samiappan S, Turnage G, Hathcock L, Casagrande L, Stinson P, Moorhead R. Using unmanned aerial vehicles for high-resolution remote sensing to map invasive Phragmites australis in coastal wetlands. Int J Remote Sens. 2017;38:2199–217.

47. Government of Western Australia Drones Improve Invasive Weed Surveillance. https://www.agric.wa.gov.au/news/media-releases/drones-improve-invasive-weed-surveillance (accessed on 21 December 2021).

48. Zaman B, Jensen AM, McKee M. Use of high-resolution multispectral imagery acquired with an autonomous unmanned aerial vehicle to quantify the spread of an invasive wetlands species. In: Proceedings of the 2011 IEEE International Geoscience and Remote Sensing Symposium; Vancouver, BC, Canada; 2011. p. 803–6.

49. Liu M, Yu T, Gu X, Sun Z, Yang J, Zhang Z, et al. The impact of spatial resolution on the classification of vegetation types in highly fragmented planting areas based on unmanned aerial vehicle hyperspectral images. Remote Sens. 2020;12:146.

© 2026 The Author(s). | Published by Agro Intelligence Research Press